Automated Medical Image Segmentation Using a New Deformable Surface Model

Suhuai Luo

The University of Newcastle, Australia

Summary
This paper introduces an automated medical image segmentation algorithm which can be used to locate volumetric objects such as brain tumor in Magnetic Resonance Imaging (MRI) images. The algorithm is novel in that it deals with MRI slices (or images) as a three dimension (3D) object as a whole. All the processes of segmentation are done in 3D space. First, it removes noisy voxels with 3D nonlinear anisotropic filtering. The filtering well preserves the intensity distribution continuity in all three directions as well as smoothes noisy voxels. Second, it uses a novel deformable surface model to segment an object from the MRI. A dynamic gradient vector flow is used in forming the surface model. Experiments have been done on segmenting tumors from real MRI data of human head. Accurate 3D tumor segmentation has been achieved.

Key words:
segmentation, anisotropic filtering, deformable surface model

1. Introduction

Magnetic Resonance Imaging (MRI) uses magnetic resonance to produce body images with high spatial resolution and excellent discrimination of soft tissues. Automatically segmenting tissues and organs from MRI images represents a particularly challenging problem due to the complexity and variability of human anatomy. There has been a substantial amount of research on automated segmenting tissues and organs from MRI images [1, 2, 3, 4, 5, 6]. Of all the MRI segmentation techniques, there are two major approaches, namely (a) region-based approach which searches for regions satisfying a given homogeneity criterion, and (b) edge-based approach that searches for edges among regions with different characteristics.

Hybrid strategies have also appeared in recent years. Notably active contour models, known as "snakes", have been widely studied and applied in medical image segmentation. Their applications include edge detection, segmentation of objects, shape modelling and motion tracking. Snakes were first introduced in 1987 by Kass *et al.* [7]. They generally represent an object boundary as a parameter curve or surface. An energy function is associated with the curve, so the problem of finding an object boundary is cast as an energy minimisation process. Typically, the curves are affected by both an internal force and external force. A snake can locate object contours well, once an appropriate initialisation is done. However, since the energy minimisation is carried out locally, the located contours can be trapped by a local minimum. A number of methods have been proposed to improve the snake's performance [8, 9]. Recently, a gradient vector flow (GVF)-based deformable model has been proposed [10]. Instead of directly using image gradients as an external force, it uses a spatial diffusion of the gradient of an edge map of the image. GVF snake was proposed to address the traditional snake's problems of short capture range and inability to track at boundary concavity. But GVF still may not be able to capture object contours in some medical image segmentation. Efforts at improving the original GVF snake's performance have been published recently. Xu *et al.* combined GVF force with a constrained balloon force to segment gyri in the cortex [11]. Although this combination works well on this case, its requirement of an *a priori* knowledge of the region of interest may restrict its application. Yu *et al.* proposed to compute the GVF using a polar coordinate representation instead of Cartesian coordinates [12]. In this way, the method can perform better than the original GVF snake in areas of long thin boundary concavities and boundary gaps. But the capture range of this improved GVF does not seem larger than the original method.

2. Automated Segmentation Using Deformable Surface Model

2.1 Principles

MRI data is acquired by scanning the object slice by slice. A major issue may hinder the effort of any automatic segmentation approach. That is the intensity inhomogeneity existed in both intrascan and interscan. There are many attempts to correct these intensity inhomogeneities [13]. Our consideration of alleviating the influence of intensity inhomogeneity on segmentation is embedded into two stages. First, a 3D nonlinear anisotropic filter is designed to smooth noisy voxels yet preserve intensity distribution continuity and edge sharpness in all three directions. Then a deformable surface model that evolves in 3D space is developed to segment an object from MRI data. A dynamic gradient vector flow is used in forming the surface model. The rest of this section is devoted to the detailed discussion of the approach.

2.2 Nonlinear Anisotropic Filtering

A first step in processing a noise-affected image is to smooth the image with Gaussian function. Basic effects of a Gaussian filtering are smoothing the image and wiping off noisy pixels or voxels. For applications where gradient operations are needed to derive edge information, a Laplacian operation will follow the Gaussian operation. These two operations are usually called Laplacian of Gaussian (LoG). In our deformable surface model, a 3D edge map is needed to form dynamic gradient vector flow. However, since the LoG operation is isotropic, sharpness of edges will also be smoothed. Therefore our goal is to find a filtering operation which can both preserve edge structures and smooth noisy background voxels. One such solution is in nonlinear anisotropic diffusion [14].

Considering specific requirements in 3D MRI segmentation, we use a nonlinear anisotropic diffusion function as described by EQ. (1).

$$\frac{\partial}{\partial t} I(x, y, z, t) = div(f(\nabla I)\nabla I) \qquad (1)$$

Where $I(x,y,z,t)$ is the voxel intensity value, $f(\nabla I)$ is a dilation function of gradient described by EQ. (2).

$$f(\nabla I) = 1/(1 + k \bullet |\nabla I(x, y, z, t)|) \qquad (2)$$

Where, parameter k decides the effect of diffusion. With very low k value, diffusion will happen across edges. While with very high k value, diffusion will need more iterations.

The effect of nonlinear anisotropic filtering can be observed from Fig.1. In the figure, the top image is an axial slice of MRI brain images. The middle image is the corresponding output of nonlinear anisotropic filtering. Though no apparent difference between the two images can be perceived by eyes, the advantages of the filtering can be observed by checking the intensity distribution of a particular row before and after the filtering. The bottom figure gives the intensity distribution of the top image at the 110th row (red curve) and the intensity distribution of

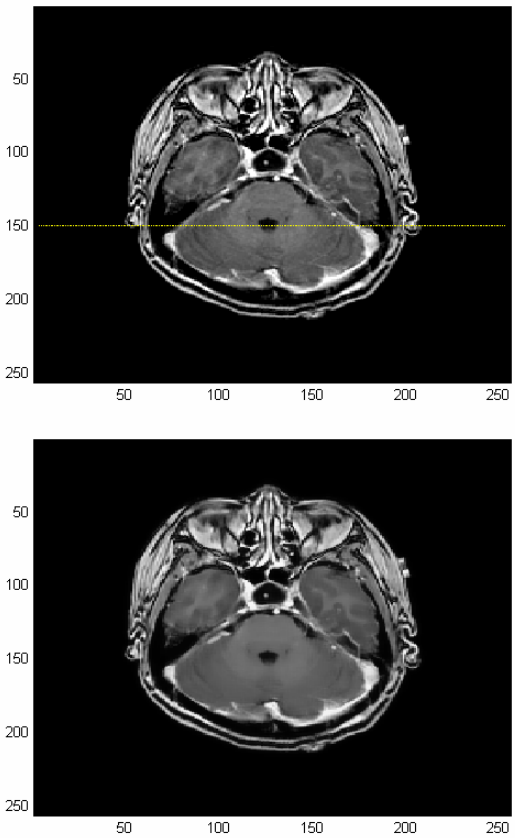

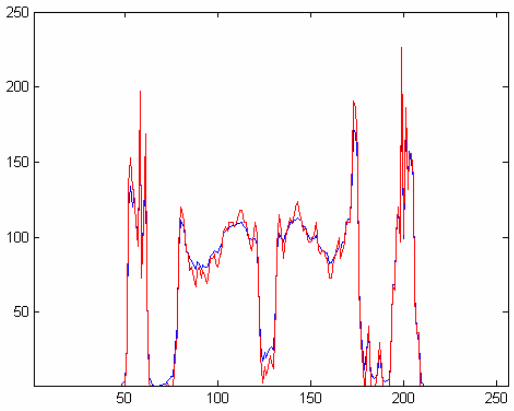

Fig.1 An example of nonlinear anisotropic filtering on an MRI brain image

Top: an original MRI brain image. The yellow line indicates the position of the 150th row.

Middle: nonlinear anisotropic filtered result of the original image

Bottom: illustration of the nonlinear anisotropic filtering effect on the 150th row of the image. The red curve indicates the intensity distribution of the original image; the blue curve indicates that of the corresponding filtered row.

Note: the numbers on x-axes represent pixel position horizontally; the numbers on y-axes represent pixel position vertically in the top and middle images, and pixel intensities in the bottom figure.

intensity distribution curves, it can be easily seen that the nonlinear anisotropic filtering preserved the edge structures as well as smoothed out noise.

2.3 Deformable Surface Model

This section describes the mathematic formulation of our deformable surface model, including the principles of snakes, adaptive balloon force, GVF force, and dynamic GVF snakes.

2.3.1 Snakes in 3D

A 3D snake is a surface $C(s) = (x(s), y(s), z(s))$, where $s \in [0,1]$. The surface moves through the image space to minimize a specified energy function. In traditional snakes, the energy is usually formed by internal forces and external forces as described in equation (3).

$$E_{snake} = E_{\text{int}} + E_{ext} \tag{3}$$

E_{int} tends to elastically hold the surface together (elasticity forces) and to keep it from bending too much (bending forces). This energy is defined in equation (4).

$$E_{\text{int}} = \frac{1}{2}\int_s \alpha |C_s|^2 ds + \frac{1}{2}\int_s \beta |C_{ss}|^2 ds \tag{4}$$

Where C_s and C_{ss} represent the first and second derivative respectively. We can control the snake's tension and rigidity by adjusting the coefficients α and β.

The external force E_{ext} intends to pull or push the surface towards the edges. Typically, it consists of potential forces. Depending on the consisting components of the external force, snakes with different performances are formed.

2.3.2 Dynamic GVF Snakes

We have developed a 3D dynamic GVF snake to segment MRI data. The snake is formed mainly by using an adaptive balloon force and a dynamic GVF force.

adaptive balloon force

A balloon model as a pressure force can be added to snake as a second external force to push the surface outward or inward [15]. In this way, the surface is considered as a balloon that has been inflated or deflated. Equation (5) represents the pressure force $f_p(s)$, where m is the amplitude of the force and $\vec{n}(s)$ normal unit vector to the curve at point C_s.

$$f_p(s) = m\vec{n}(s) \tag{5}$$

The balloon force is considered to increase the capture range of the image potential force. This is a proper consideration given that the snake can be set to start evolving inside the object. Unfortunately, balloon force introduces unpredictability to the performance of the active surface and makes it more sensitive to the values of its different parameters. To overcome the unpredictability problem introduced by the balloon force, we apply this force in an adaptive way. The main idea is to give the balloon force bigger weight compared to the GVF force at the early stage of the evolution, and to give the balloon force smaller weight at the later stage. In this way, the speed of the convergence is increased, and the snake can be correctly pushed toward the surface even if it starts far away with less chance of being over-pushed.

GVF force

Gradient vector flow force was proposed as a new external force to achieve better object segmentation [10]. Its basic idea is to extend influence range of image force to a larger area by generating a GVF field. The GVF field is computed from the image. In detail, a GVF field is defined as a vector field ***V*** that minimizes the energy function *Q*. *Q* is described in equation (6).

$$Q = \iiint \mu \nabla^2 V + |\nabla f|^2 |V - \nabla f|^2 \, dxdydz \quad (6)$$

Where, *f* is the edge map which is derived by using an edge detector on the original image space, and μ is a regularization parameter. Using variational calculus, the GVF field can be obtained by solving the corresponding Euler-Lagrange equations.

Fig. 2 illustrates the GVF force distribution of an ellipse in 2D. Where, the force is represented by a vector with direction and value. It can be observed that the GVF force points to the ellipse curve.

dynamic GVF force

We have developed a dynamic GVF force to provide a unique evolution-stop mechanism as well as all the characteristics owned by the original GVF force. The evolution-stop mechanism is needed to prevent the snake from breaking through the correct surface and locking to other feature points. The breakage can happen in areas where two objects or organs are very close to each other. The introduction of the dynamic GVF force is inspired by a property of the GVF field. That is, when the GVF field passes a surface, its direction will change. A consistency degree is incorporated into the new dynamic GVF force. The force varies according to the consistency. If the evolution of the snake will cause the change of GVF force direction, it is said inconsistency has occurred and the snake is not allowed to evolve to the new position.

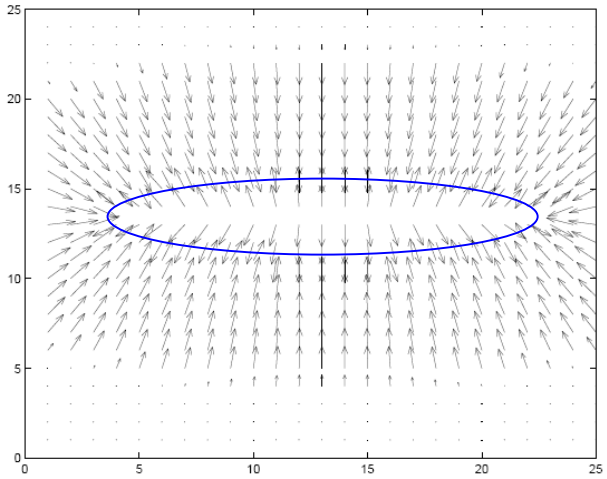

Fig. 2 An example of GVF field of an ellipse image

Note: the blue ellipse curve indicates the position of the ellipse in the original image out of which this GVF field is derived. The GVF forces are represented as vectors with directions and values.

3D dynamic GVF snake

With the inclusions of the adaptive balloon force and the dynamic GVF force, the evolution of the snake can be derived by solving equation (3). The equation can be solved by using variational calculus and the Euler-Lagrange differential equation. Then, the solution to this force balance, as defined in equation (7), represents the snake's final position.

$$\alpha C_{ss} - \beta C_{ssss} + \gamma V_{dyn} + \lambda f_{pa} = 0 \quad (7)$$

Where f_{pa} is the adaptive balloon force; V_{dyn} is the dynamic gradient vector flow force as defined in equation (8).

$$V_{dyn} = \begin{cases} V & \text{if} \quad C_\theta \geq T_\theta \\ (-\alpha C_{ss} + \beta C_{ssss} - \lambda f_{pa})/\gamma & \text{otherwise} \end{cases} \quad (8)$$

In order to explain equation (8), let x_1 be a point on the current snake and x_2 its possible next position in the evolution process. C_θ defines the consistency angle and is proportional to the angle between the GVF vectors at x_1 and x_2. T_θ represents the cut-off angle. Based on our

experiments, $T_\theta = 20^0$ is a good threshold.

The new dynamic GVF force will be the same as conventional GVF if the snake point moves towards the contour. But when the snake point tries to cross over an edge, the dynamic gradient vector flow force will stop the point from moving. The threshold T_θ will decide when this evolution-stop mechanism will be triggered.

3. Experiments and Results

In order to validate the performance of the proposed method, we applied it on magnetic resonance images of several anonymous brain tumor patients. The data are MR images in the axial plane, with 256 x 256 x 113 voxels and 1mm x 1mm x 1mm voxel resolution.

Fig. 3 demonstrates the tumor segmentation performance of our method. In the experiment, the snake parameters were chosen as: α = 0.6, β = 0.7, λ =0.3, and γ =0.4. The model was initialised with a ball of radius 5 voxels.

Fig. 3 (a) gives the initial ball's position on an axial slice. It can be seen that the initial ball is well inside the tumor area. To illustrate its performance in 3D, the segmentation results on three different slices of one subject are presented. Fig. 3(b) shows axial view of the 45th slice and corresponding segmentation result. Fig. 3(c) shows the view of the 49th slice and corresponding segmentation result. Fig. 3(d) shows the view of the 52th slice and corresponding segmentation result. In the figures, the red contours along the tumor (white) areas are the segmentation results of the proposed deformable surface model.

From the figures it can be seen that the algorithm can locate the volumetric tumor with accuracy. Comparing to the 2 dimensional approach described in [4], this new algorithm uses 3 dimensional information and has the advantages of both smoothly segmenting the tumor in the space and much less initialising work. Here the initialization involves only indicating the position and radius of an initial ball. It has less restriction on the automation of the segmentation process.

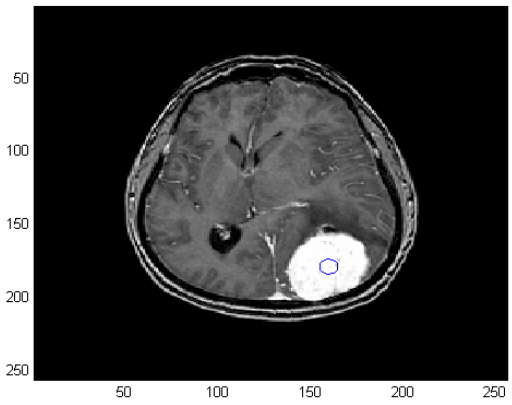

Fig. 3(a) the model's initial position (the blue circle) on an axial slice

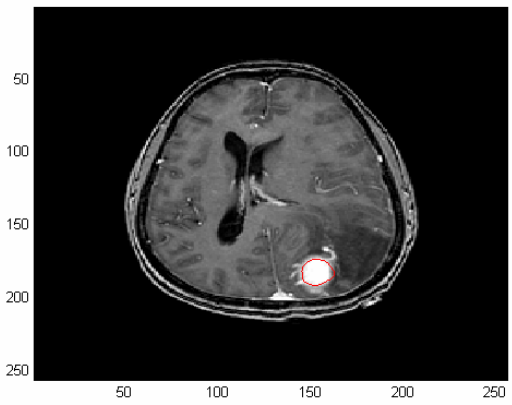

Fig. 3(b) the 45th slice and corresponding segmentation result (red contour)

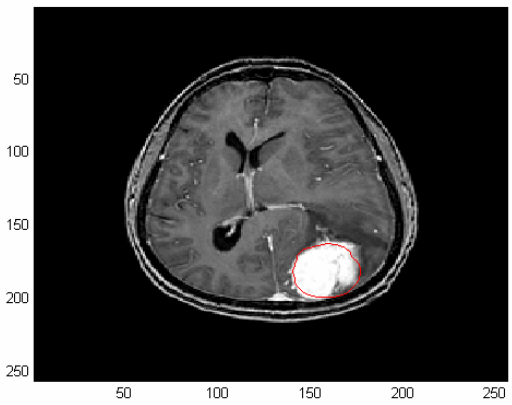

Fig. 3(c) the 49th slice and corresponding segmentation result (red contour)

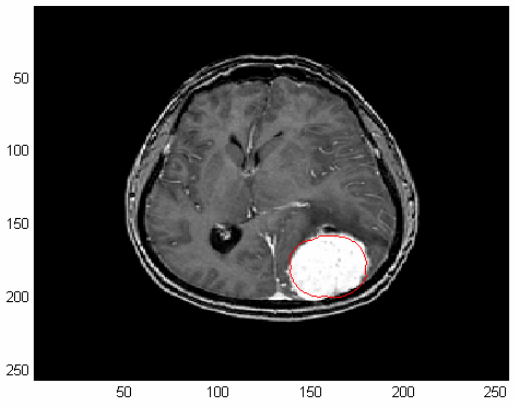

Fig. 3(d) the 52th slice and corresponding segmentation result (red contour)

Fig. 3 The results of brain tumor segmentation on MRI using the proposed deformable surface model

4. Conclusions

In this paper, we have presented a new deformable surface model for automated segmentation. It can segment objects from medical images such as MRI. In developing the algorithm, emphasis was put on considering the whole MRI data set as a 3D entity. Therefore all the processes of segmentation are done in 3D space. Two major stages were developed to segment 3D object. First, it removes noisy voxels with 3D nonlinear anisotropic filtering. The filtering well preserves the intensity distribution continuity in all three directions as well as gets rid of noisy voxels. Second, it uses a deformable surface model to segment an object from the MRI. A dynamic gradient vector flow is used in forming the surface model.

Real MRI data were used to evaluate the segmentation performance. Especially, brain tumor segmentation from MRI images was tested. The experiments have demonstrated the potential of our approach. The proposed segmentation method is also applicable to other applications such as blood vessel segmentation.

During developing the segmentation method, we noticed that much computation is needed because the data is huge with three dimensions. Therefore further work on the approach would be finding efficient calculation of components such as 3D gradient vector flow and snake evolving.

5. References

[1] Inomata, T., Muragaki, Y., Iseki, H., Dohi, T., and Hata, N., Intraoperative segmentation of brain tumors for open MRI guided glioma surgery, *Proc. of the 18th International Congress and Exibition, Computer Assisted Radiology and Surgery*, pp.1284, Chicago, USA, 2004.

[2] Amini, L., Soltanian-Zadeh, H., Lucas, C., and Gity, M., Automatic segmentation of thalamus from brain MRI integrating fuzzy clustering and dynamic contours, *IEEE Transactions on Biomedical Engineering*, Vol: 51, No. 5, pp. 800-811, May 2004.

[3] Boscolo, R., Brown, M. S., and McNitt-Gray, M. F., medical image segmentation using knowledge-guided robust active contours, *Radiographics*, 22(2): 437-48, 2002.

[4] Luo, S., and Li, R., A new deformable model using dynamic gradient vector flow and adaptive balloon forces, *APRS Workshop on Digital Image Computing*, Brisbane, Australia, pp. 9-14., Feb. 7, 2003.

[5] Jimenez-Alaniz, J.R. Medina-Banuelos, V. Yanez-Suarez, O., Data-driven brain MRI segmentation supported on edge confidence and a priori tissue information, IEEE Transactions on Medical Imaging, Vol. 25, Issue 1, pp. 74-83, 2006.

[6] Kobashi, S., Fujiki, Y., Matsui, M., Inoue, N., Kondo, K., Hata, Y., Sawada, T., Interactive segmentation of the cerebral lobes with fuzzy inference in 3T MR images, IEEE Transactions on Syatem, Man and Cybernetics, Vol. 36, Issue 1, pp. 74-86, Feb. 2006.

[7] Kass, M., Witkin, M., and Terzopoulos, D., Snakes: active contour models. *International Journal of Vision*, 1:321–331, 1987.

[8] McInerney, T., and Terzopoulos, D., Deformable models in medical image analysis: A survey, *Medical Image Analysis*, 1(2):91–108, 1996.

[9] Jain, A., Zhong, , Y., and Dubuisson-Jolly, M., Deformable template models: A review. *Signal Processing*, 71:109–129, 1998.

[10] Xu, C., and Prince, J., Snakes, shapes, and gradient vector flow. *IEEE Transactions on Images Processing*, 7(3):359–369, 1998.

[11] Xu, C., Pham, D., Rettmann, M., Yu, D., and Prince, J., Reconstruction of the human cerebral cortex from magnetic resonance images. *IEEE Transactions on Medical Imaging*, 18(6):467–479, June 1999.

[12] Yu, Z., and Bajaj, C., Image Segmentation Using Gradient Vector Diffusion and Region Merging, *ICPR'02*, Quebec City, pp. 828–831, August 11-15, 2001.

[13] Wells, W. M., Grimson, W. E. L., et al, Adaptive segmentation of MRI data, *IEEE Transactions on Medical Imaging*, Vol. 15, No. 4, August, pp.429-442, 1996.

[14] Weickert, J., *Anisotropic Diffusion in Image Processing*, B. G. Teubner Stuttgart, 1998.

[15] Cohen, L., and Cohen, I.., Finite-element methods for active contour models and balloons for 2-d and 3-d images. *IEEE Transactions on Pattern Analysis and Machine Intelligence*, 15(11):1146–1131, November 1993.

Suhuai Luo received the B.E. and M.E. degrees in Radio Engineering from Nanjing University of Posts and Telecommunications China in 1982 and 1987, respectively, and PhD degree in Electrical Engineering from the University of Sydney Australia in 1995.

From 1995 to 2004, he worked as a senior research scientist with the Commonwealth Scientific and Industrial Research Organisation Australia and the Bioinformatics Institute Singapore. He is now with The University of Newcastle Australia.